International Journal of Mechanical, Industrial and Aerospace Sciences
ISSN: 2517-9950
Vol:11, No:5, 2017

Optimization of the Aerodynamic Performances of an Unmanned Aerial Vehicle

Fares Senouci, Bachir Imine

***Abstract*—**This document provides numerical and experimental optimization of the aerodynamic performance of a drone equipped with three types of horizontal stabilizer. To build this optimal configuration, an experimental and numerical study was conducted on three parameters: the geometry of the stabilizer (horizontal form or reverse V form), the position of the horizontal stabilizer (up or down), and the landing gear position (closed or open). The results show that up-stabilizer position with respect to the horizontal plane of the fuselage provides better aerodynamic performance, and that the landing gear increases the lift in the zone of stability, that is to say where the flow is not separated.

***Keywords*—**Aerodynamics, wind tunnel, turbulence model, lift, drag.

I. Introduction

THE stability and aerodynamic performance of the aircraft are based on several parameters. Among these parameters, the stabilizer plays a major role on the maneuverability and the pitch and yaw control and the landing gear may present a brake on the advancement. Such importance is significant in several phases of flight (takeoff, landing, maneuvering, etc.) with well-known consequences: increased drag, partial or total loss of control of the aircraft [1], [2], etc.

This work presents a numerical and experimental study of a subsonic flow around a drone of four configurations: Unmanned Aerial Vehicle (UAV) with reverse V form stabilizer, drone with horizontal stabilizer up position, drone with horizontal stabilizer down position, and a drone with landing gear (Figs. 1-3) [3]. The first phase of this work is to build a prototype on SolidWorks to be exported to a mesh generator where a computational domain is discretized. A computer code is used to estimate the lift and drag coefficients at a speed of 20 m/s. The Spalart-Allmaras turbulence model is used to solve the Navier-Stokes equations [4]. The second phase consists of building a model of a 1/7-scale corresponding to the dimensions of the test vein of the wind tunnel. The tests in the wind tunnel are conducted at a 20 m/s speed for an angle of attack variation from 5° to 17° to determine the lift and drag coefficients. The wind tunnel tests and the numerical tests were effectuated and compared with each other. These experiments allowed us to bring out the main trends in order to obtain an optimal design and to validate a mathematical model.

Fares Senouci is with the Oran University of Science and Technology-Mohamed Boudiaf, Algeria (e-mail: senouci.fares41@gmail.com).

II. Description of UAVs

The first drone is shown in Fig. 1. It has a 0.64-m wingspan and swept wing of 3.5° a dihedral of 4° and an empennage of NACA 0012 in reverse V form, and a 0.035-m^2 area and a 0.65-m chord.

Fig. 1 UAV with landing gear

The second drone is shown in Fig. 2. It is a UAV without landing gear it has an up-horizontal stabilizer. It has a 0.64 m wingspan and swept wing of 3.5° a dihedral of 4° and an empennage of NACA 0012 in reverse V form, and a 0.035-m^2 area and a 0.65-m chord.

Fig. 2 UAV with an up-horizontal stabilizer and without landing gear

Fig. 3 UAV with a down-horizontal stabilizer and without landing gear

The third UAV is shown in Fig. 3. It is a UAV without landing gear and it has a down-horizontal stabilizer. It has a 0.64-m wingspan and swept wing of 3.5° a dihedral of 4° and

an empennage of NACA 0012 in reverse V form, and a 0.035-m^2 area and a 0.65-m chord.

III. Transport Equation and Turbulence Model

The flow around the UAV is considered turbulent and symmetric. The general form of the transport equations can be written in Cartesian coordinates as follows:

The continuity equation in its general form:

$$\frac{\partial}{\partial xj}\left(\overline{\rho}\widetilde{U}j\right) = 0 \quad (1)$$

And the conservation equation of the moment in its general form:

$$\frac{\partial}{\partial x_j}\left(\overline{\rho}\widetilde{U}i\widetilde{U}j\right) = \overline{\rho}\, g_i - \frac{\partial \overline{p}}{\partial x_i} - \frac{\partial}{\partial x_j}\left(\rho\tilde{u}_i\tilde{u}_j\right) + \frac{\partial}{\partial x_j}\left[\overline{\mu}\left(\frac{\partial \widetilde{U}i}{\partial x_j} + \frac{\partial \widetilde{U}j}{\partial x_i}\right) - \frac{2}{3}\overline{\mu}\frac{\partial}{\partial x_k}\delta ij\right] \quad (2)$$

where U is the flow velocity.

Turbulence Model [4]: The turbulence model used in this work is a model with a transport equation for the quantity suggested by Spalart and Allmaras.

$$\frac{\partial(\overline{\rho}\overline{\vartheta})}{\partial t} + \vec{\nabla}.\left(\overline{\rho}\,\vec{V}\hat{v}\right) = \vec{\nabla}.\left[\frac{\overline{\mu}+\overline{\rho}\,\tilde{v}}{\partial SA}\,\vec{V}\hat{v}\right] + \mathrm{P}_v - D_v \quad (3)$$

where the terms of production and destruction are defined as:

$$P_v = C_{b1}C_\mu\tilde{S}\bar{\rho}\tilde{v} + C_{b2}\frac{\overline{\rho}\left(\vec{\nabla}\vec{v}\right)^2}{\partial SA} \quad (4)$$

$$D_v = C_{w1}f_w\frac{\overline{\rho}\left(\vec{\nabla}\vec{v}\right)^2}{\rho d^2} \quad (5)$$

$$f_x = \mathrm{g}\left(\frac{1+C_{W3}^6}{\mathrm{g}^6+C_{W3}^6}\right) \quad (6)$$

with $\mathrm{g} = r + C_{w2}(r^2 - r)$ and

$$M_t = \bar{\rho}\tilde{v}\frac{x^3}{x^{3+}C_{v1}} \qquad x = \frac{\bar{\rho}\tilde{v}}{\mu} \quad (7)$$

The closing coefficients are given by the following values:

$$\sigma SA = \frac{2}{3}\,;\; C_{b1} = 0.1355\,;\; C_{b2} = 0.622 \quad (8)$$

$$C_{v1} = 7.1\,;\; C_{w1} = 0.3\,;\; C_{w3} = 2 \quad (9)$$

IV. Experimental Installation

The experiments were realized in a subsonic wind tunnel with closed circuit and 0.46 m × 0.46 m test section.

In the test section, the speed was fixed at 20 m/s (which corresponds to 2.10^5 Reynolds number).

The wind tunnel is horizontal type. A conventional closed-circuit wind tunnel has advantages over an open-circuit wind tunnel (Fig. 4); especially, a higher flow velocity, a lower energy consummation, and a lower noise level. The air velocity around the UAV is produced by an axial flow motor and produces a maximum velocity of 69 m/s [5]. In order to make tests in the wind tunnel, a prototype is drawn on SolidWorks to be able to produce a wooden model of a 1/7-scale and 0.425 m wingspan which corresponds to the dimensions of the test vein.

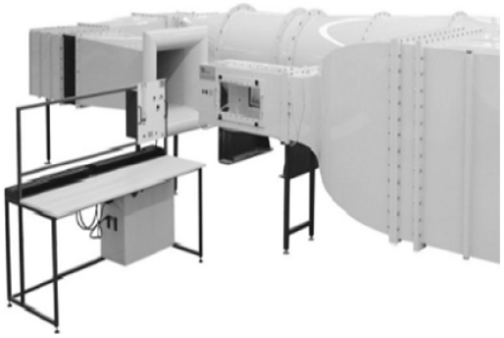

Fig. 4 Subsonic wind tunnel

Fig. 5 Model in the wind tunnel

V. Mesh and Boundary Conditions

Like most of the problems involved in fluid flow, a virtual wind tunnel is an ideal configuration. All three-dimensional problems could be divided along the longitudinal plane of symmetry [5].

After the models were imported from SolidWorks, a field was created around the UAV to analyze the flow. It is important to examine the asymmetries of the mesh elements to ensure that there are no highly asymmetric elements present in the mesh [5]. One should recall that very uneven elements can cause solution convergence problems in FLUENT [6].

The boundary conditions must be defined by GAMBIT. An initial speed condition at the input is used to define the flow velocity at the inlet. The front face of the flow control volume is imposed as an initial condition for the input speed. To specify the flow properties entering the volume or calculation domain in addition to the face before, the left, top, and bottom faces are also specified to ensure that the flow properties are taken into account by the FLUENT solver. The outflow plane is specified as an output condition of this flow. The surface of the UAV is specified as a boundary of the wall to differentiate the solid and liquid regions. Finally, the plane of symmetry is

specified as a plane of symmetry. A summary of the boundary conditions used for this UAV is shown in Fig. 7.

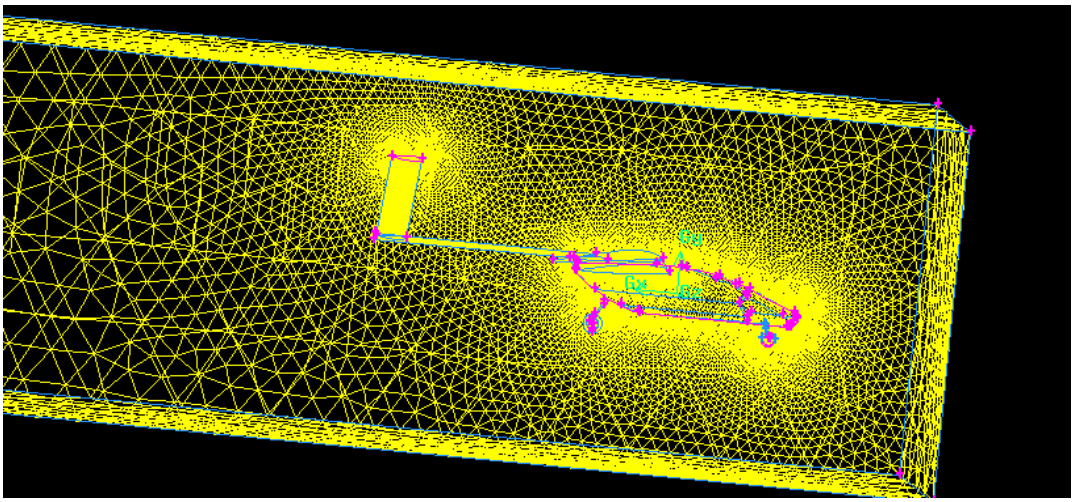

Mesh and boundary conditions

Fig. 6 The mesh landing gear UAV

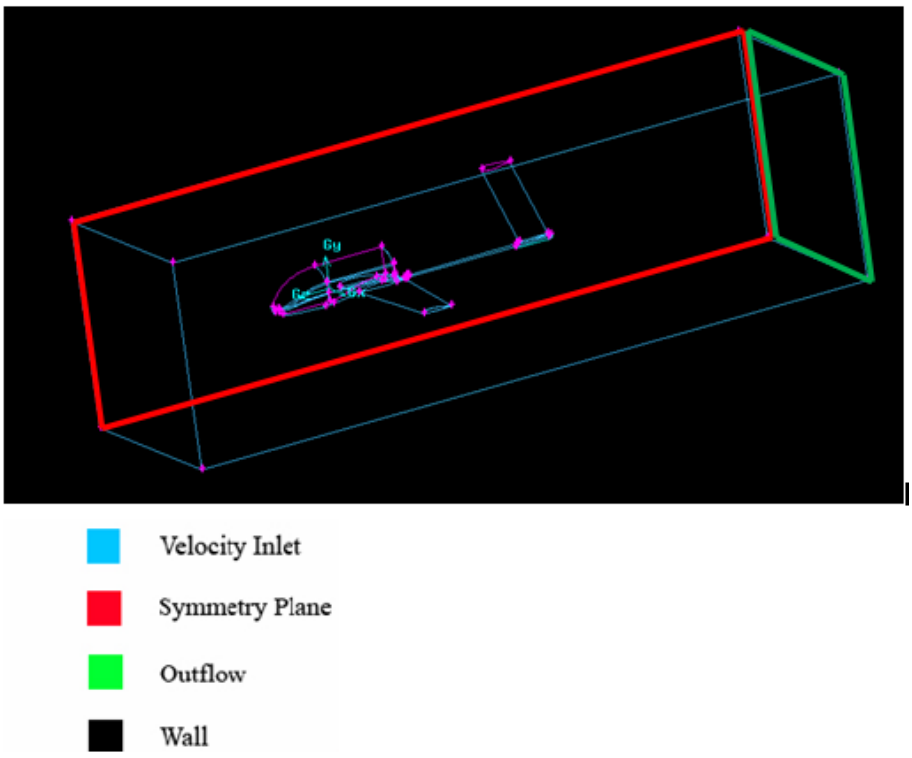

Fig. 7 Summary of boundary conditions

VI. Results and Discussions

Several results have been found for several angles of attack which varying between -5° and 17° to determine the lift and drag of the three types of UAVs for a 20-m/s air flow.

Fig. 8 compares the lift coefficients obtained numerically with that obtained experimentally for a reverse V form UAV with a landing gear. A difference of 24% is observed on the evolution of the lift in favor of the experiment and an increase of the point of stall of 4° in favor of the digital [7], it is certainly to the choice of the model of turbulence which remains imprecise in the separates flux zone.

The experimental lift coefficients comparison of UAV with

and without landing gear is shown in Fig. 9. The landing gear increases the lift in the zone where the flow is stable, while in the flow separation zone, the lift is not affected by the presence of the landing gear.

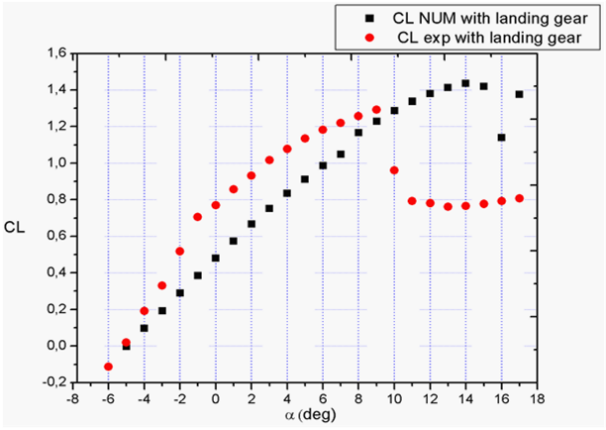

Fig. 8 Evolution of the numerical and experimental lift coefficients of the UAV with landing gear and reverse V form of stabilizer

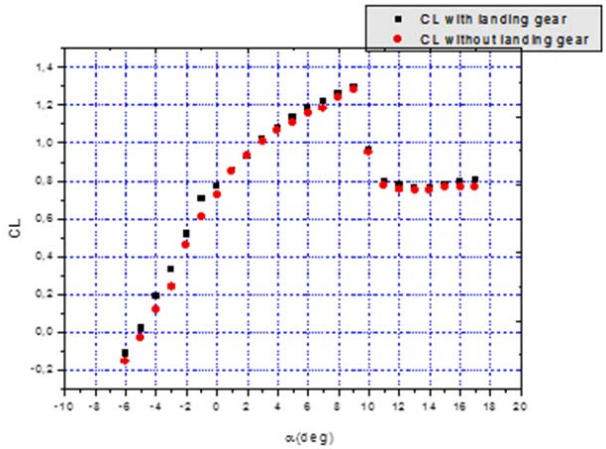

Fig. 9 Evolution of the experimental lift coefficients of the UAV with and without landing gear

The lift of the UAV with up-horizontal stabilizer is much better than the UAV with down-horizontal stabilizer. This is due to the presence of vortices generated by the fuselage and the wing which affect the down-horizontal stabilizer Fig 10.

If we compare two drones of the same category (UAV with up-horizontal stabilizer and UAV with reverse V form) as shown in Fig. 11, the up-horizontal stabilizer pushes the stall to 2 degrees.

Fig. 12 compares the drag coefficients obtained numerically with that obtained experimentally for a reverse V form of stabilizer of UAV with landing gear.

The gap is in favor of the UAV with a reversed V form of stabilizer throughout the evolution of the two curves

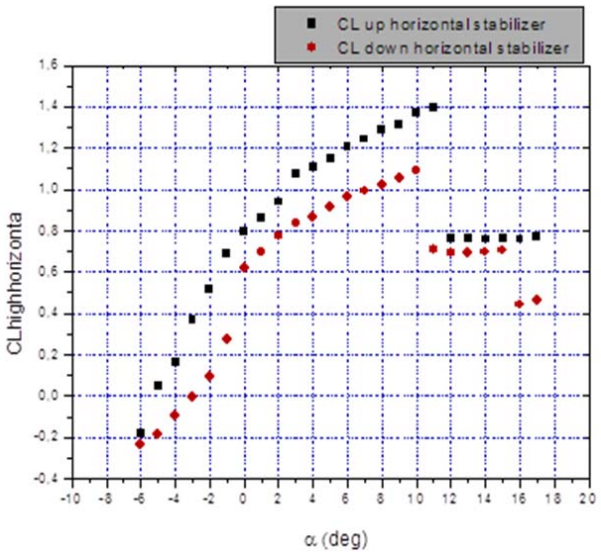

Fig. 10 Evolution of the experimental lift coefficients of the up and down-horizontal stabilizer

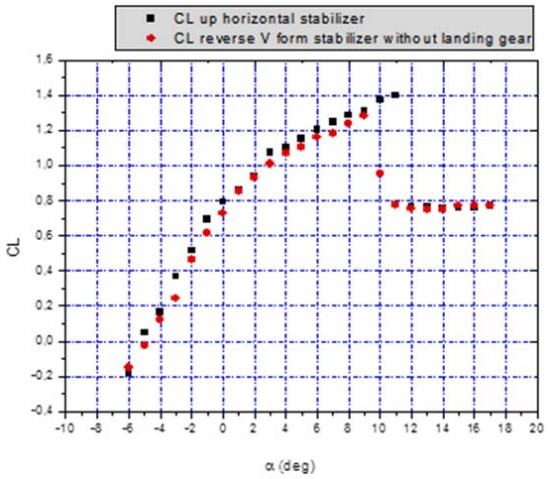

Fig. 11 Evolution of the experimental lift coefficients of the up-horizontal stabilizer and reverse V form of stabilizer

Fig. 13 represents the evolution of the experimental coefficients of drag as a function of the angle of attack of the UAV with up-horizontal stabilizer and UAV with down-horizontal stabilizer. It can be seen that the up-horizontal stabilizer has less drag than the down-horizontal stabilizer.

Fig. 14 represents the evolution of the experimental drag coefficients as a function of the angle of attack of the UAV with landing gear and of the UAV without landing gear. The landing gear represents a light braking on the advancement.

Fig. 15 compares the drag of the UAV with up-horizontal stabilizer and the UAV with reverse V stabilizer. Unlike the lift, the up-horizontal stabilizer breaks the progress of the drone compared to the UAV with reverse V stabilizer form.

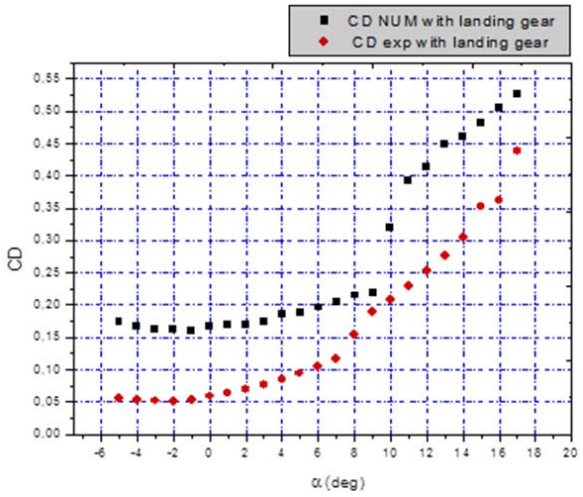

Fig. 12 Evolution of the experimental and numerical drag coefficients of the reverse V form of stabilizer for a UAV with landing gear

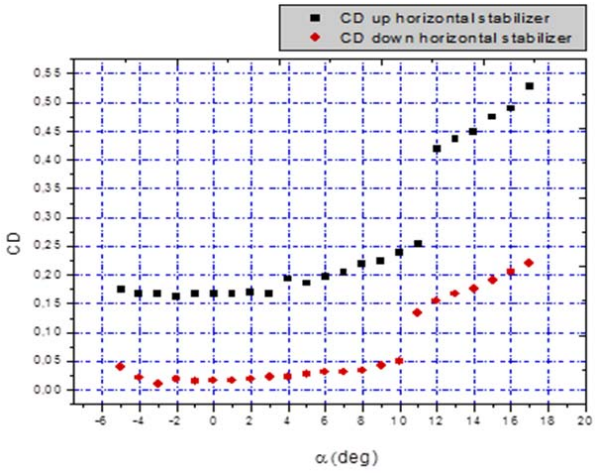

Fig. 13 Evolution of the experimental drag coefficients of up-horizontal stabilizer and down-horizontal stabilizer

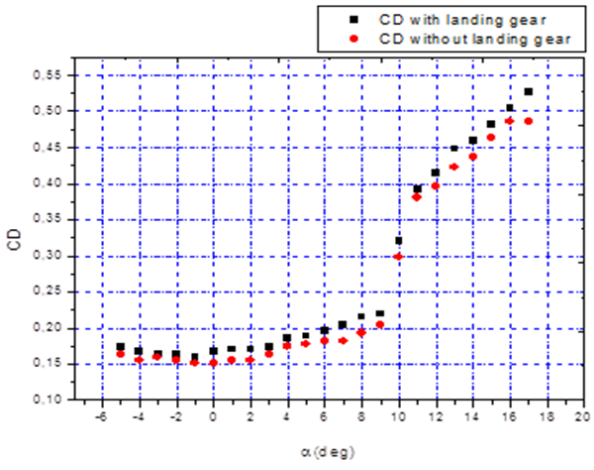

Fig. 14 Evolution of the experimental drag coefficients of reverse V form of stabilizer for an UAV with and without a landing gear

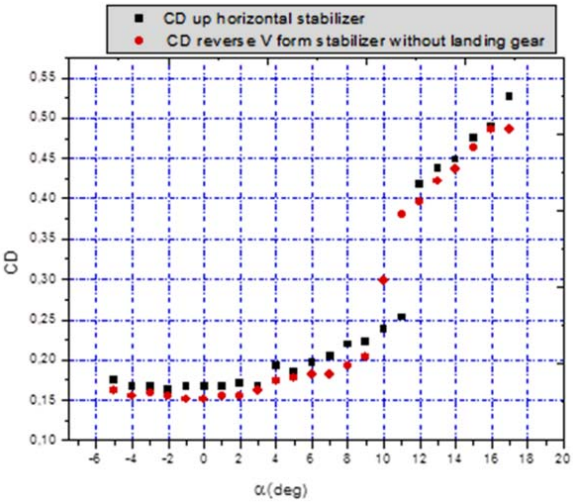

Fig. 15 Evolution of the experimental drag Coefficients of reverse V form of stabilizer for an UAV without landing gear and UAV with up-horizontal stabilizer

VII. Conclusion

This study examines the influence of stabilizer and the presence of the landing gear on the aerodynamic performance of UAVs. The study focuses on the optimization of the shape of the stabilizer (in reverse V or horizontal) and their position (up and down) and the landing gear (closed or open position). A numerical study was also conducted.

References

[1] O. M. Fouatih, et al.―Design optimization of the aerodynamic passive flow control on NACA 4415 airfoil using vortex generators‖, DOI: 10.1016/j.euromechflu, 2015.11.006.
[2] Elsa M. Cárdenas et al.―Design of an Unmanned Aerial Vehicle for Ecological Conservation‖ DOI: 10.2514/6.2005-7056·
[3] Luis Velazquez, ―low-speed wind tunnel testing for an unmanned aerial vehicle airfoil‖, Institute of Thermomechanics AS CR, v.v.i., Prague, October 21 - 23, 2009.
[4] A. Zeghib, Revue des Energies Renouvelables CISM'08 Oum El Bouaghi, 311 – 324, 2009.
[5] Manuel de la TE 44 Subsonic Wind Tunnel.
[6] Fluent 62 User's Guide. Fluent, Inc, 2005.
[7] F. Senouci, B. Imine―Numerical and Experimental Study of Flow around an UAV ‖SKP Engineering college, TN, India, 16-17, 2011, pp. 400–404, December 2011, unpublished.